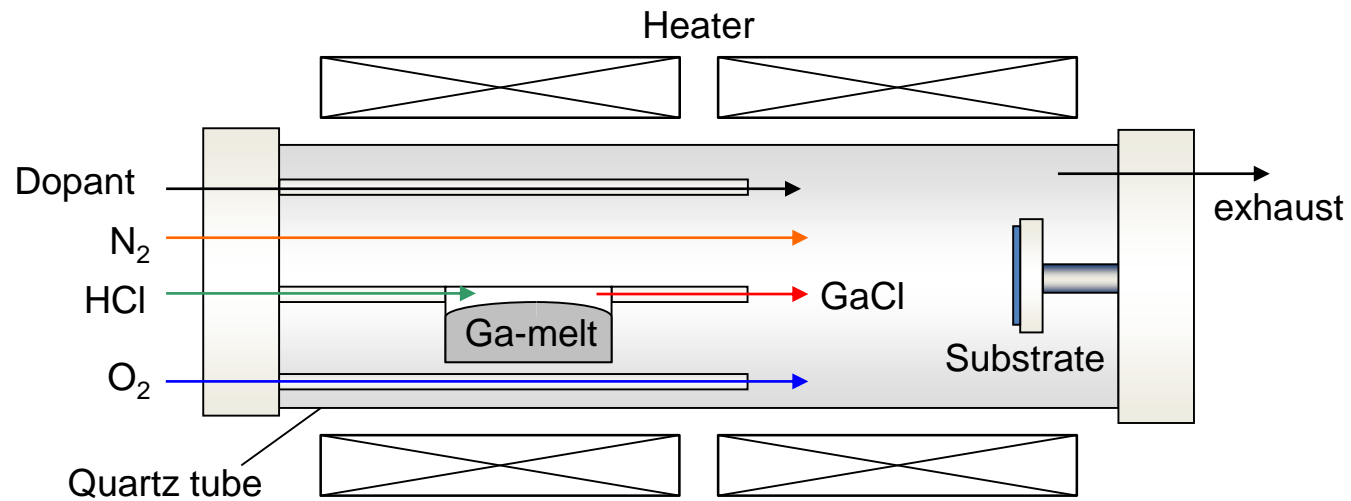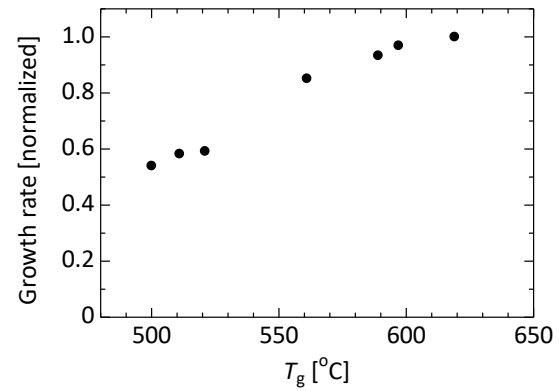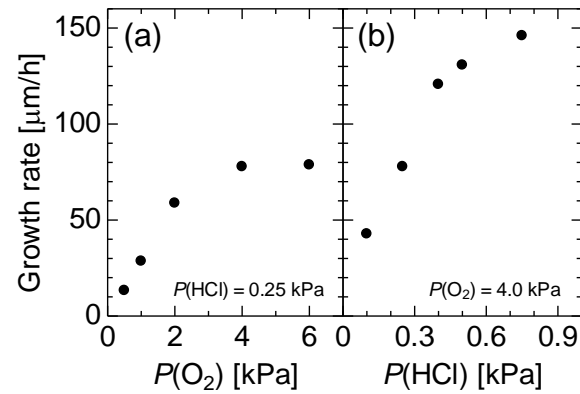Figure 1

Schematic illustration of an HVPE reactor for Ga_2O_3 .

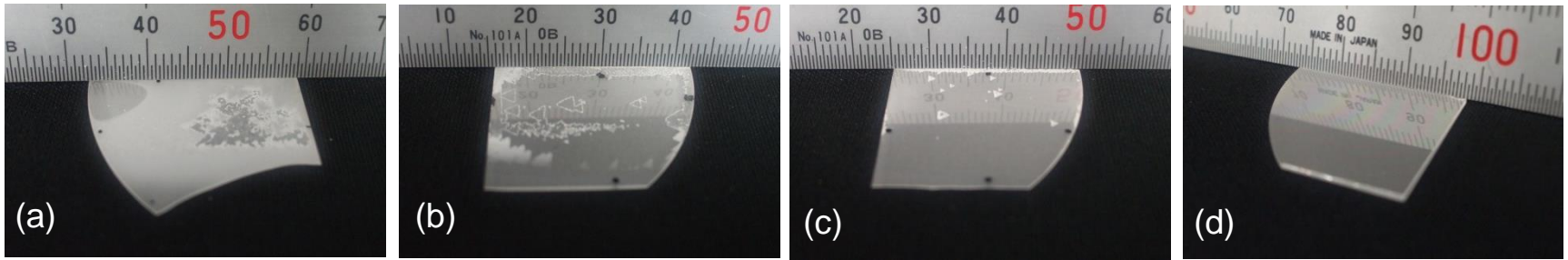Figure 2

Growth rate of α-Ga$_2$O$_3$ as a function of growth temperature.
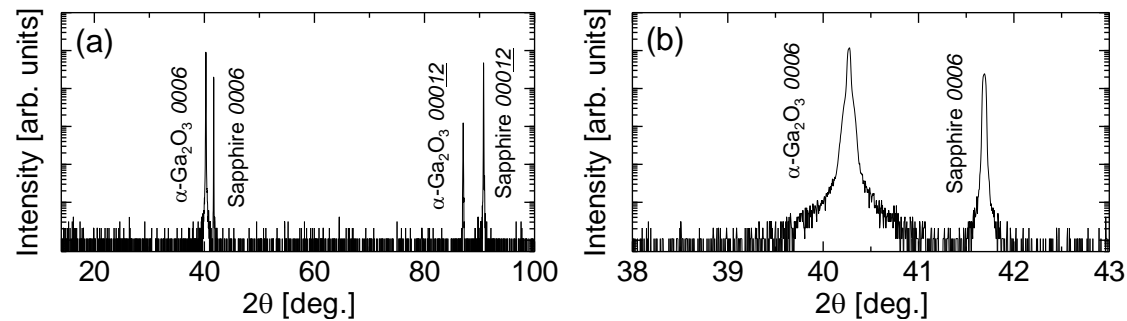
Figure 3

Growth rate of α-Ga$_2$O$_3$ as functions of (a) O$_2$ partial pressure and (b) HCl partial pressure. [8]
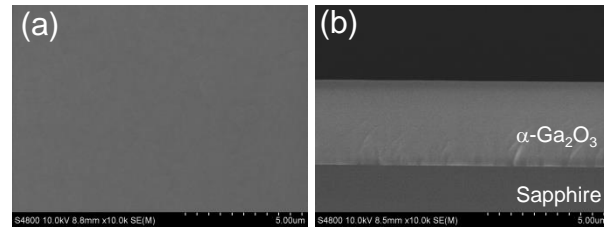
Figure 4

(a) (b) (c) (d)

Photographs of Ga_2O_3 films grown at (a) 650ºC, (b) 600ºC, (c) 575ºC, and (d) 550ºC.

Figure 5

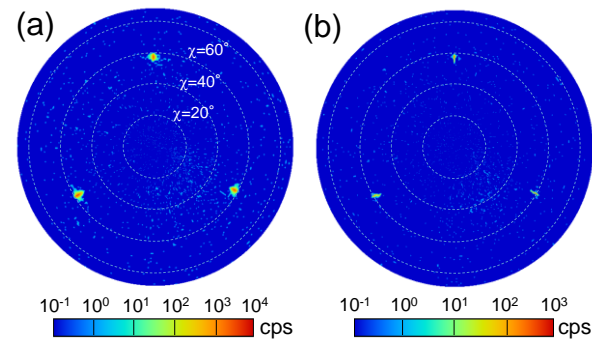XRD 2θ–ω profiles of an α-Ga$_2$O$_3$ layer: (a) wide-scan profile and (b) narrow-scan profile near *0006* diffraction. [8]
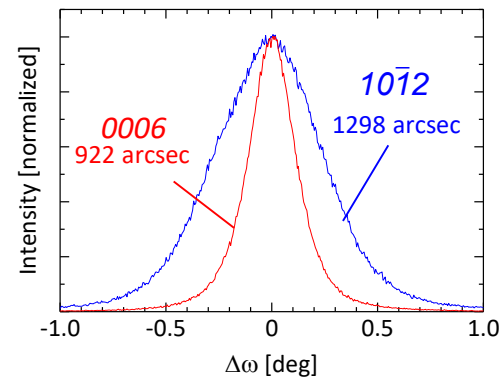
Figure 6

SEM images of an α-Ga$_2$O$_3$ layer: (a) surface image and (b) cross-sectional image. [8]
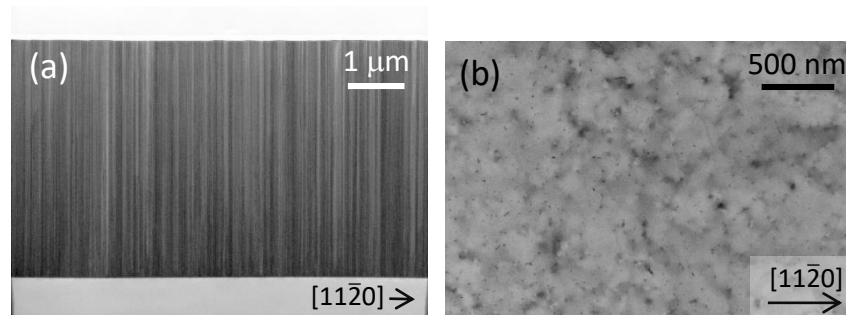
Figure 7

X-ray $10\bar{1}2$ pole figures (log scale) of (a) α-Ga$_2$O$_3$ layer and (b) sapphire substrate.
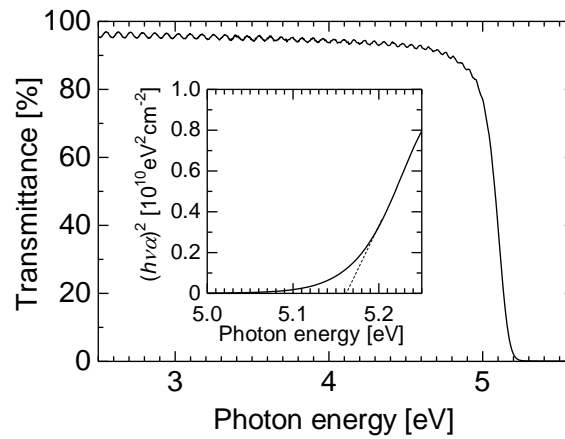
Figure 8

XRCs of a conventional α-Ga$_2$O$_3$ film grown by HVPE [8].
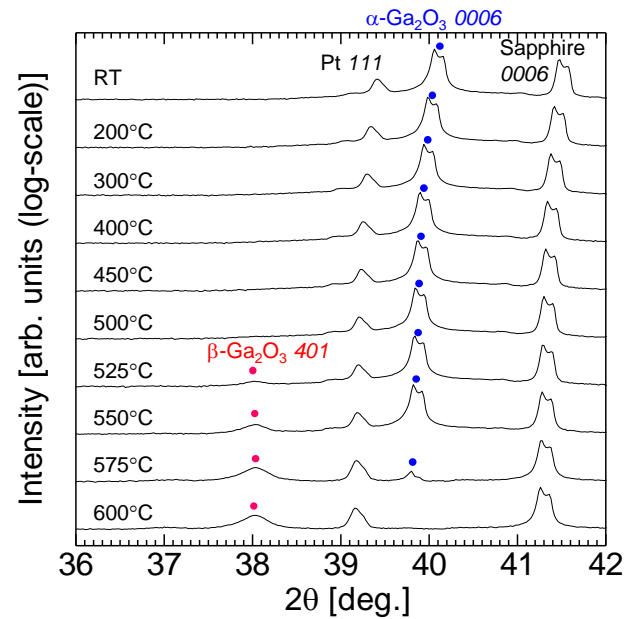
Figure 9

TEM images of a conventional α-Ga$_2$O$_3$ film grown by HVPE:
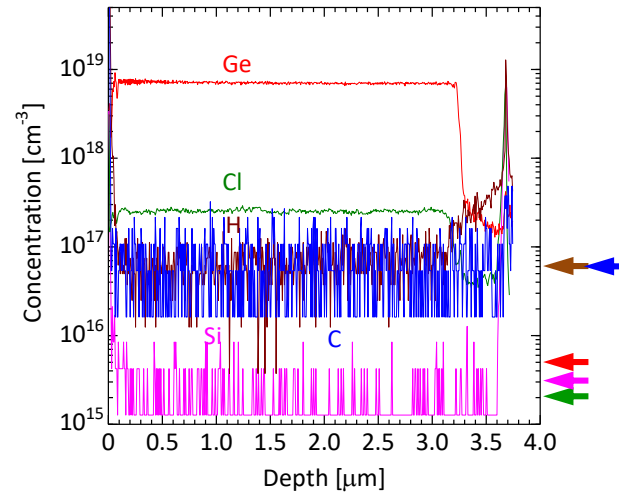(a) cross-sectional image and (b) plan-view image.

Figure 10

Transmittance spectra of α-Ga$_2$O$_3$. The inset shows the absorption coefficient in $(h\nu\alpha)^2$ vs. $h\nu$.
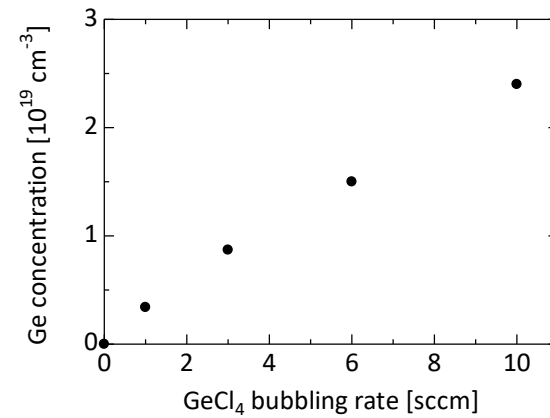
Figure 11

XRD 2θ–ω scan profiles for an HVPE-grown α-Ga$_2$O$_3$ film measured at RT and elevated temperatures.

Figure 12

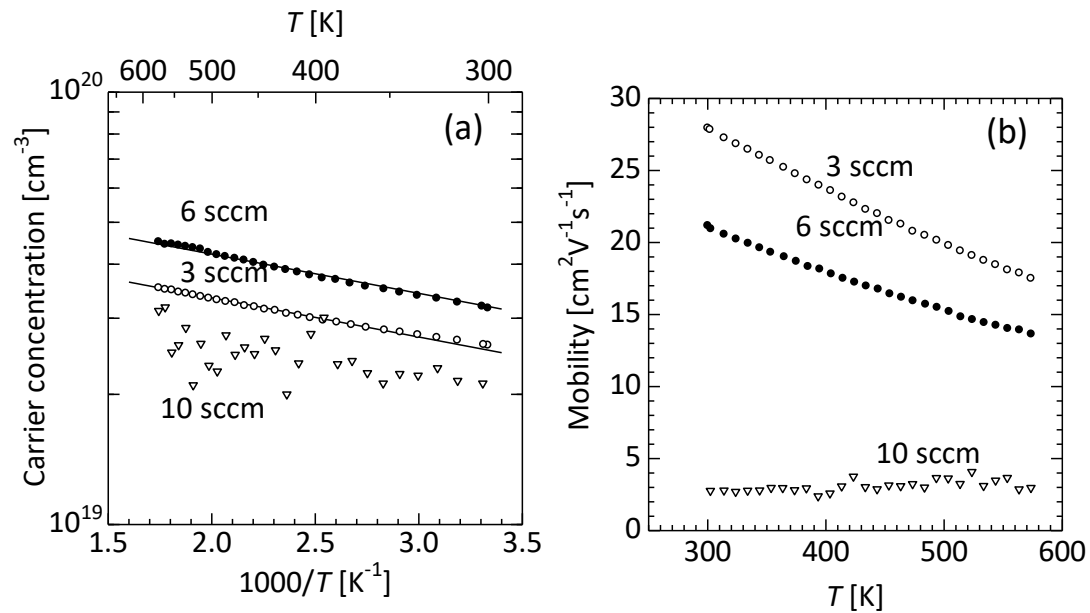SIMS depth profile of a Ge-doped α-Ga$_2$O$_3$ film. The arrows indicate the detection limits.

Figure 13

Ge concentration in α-Ga$_2$O$_3$ as a function of GeCl$_4$ bubbling rate.
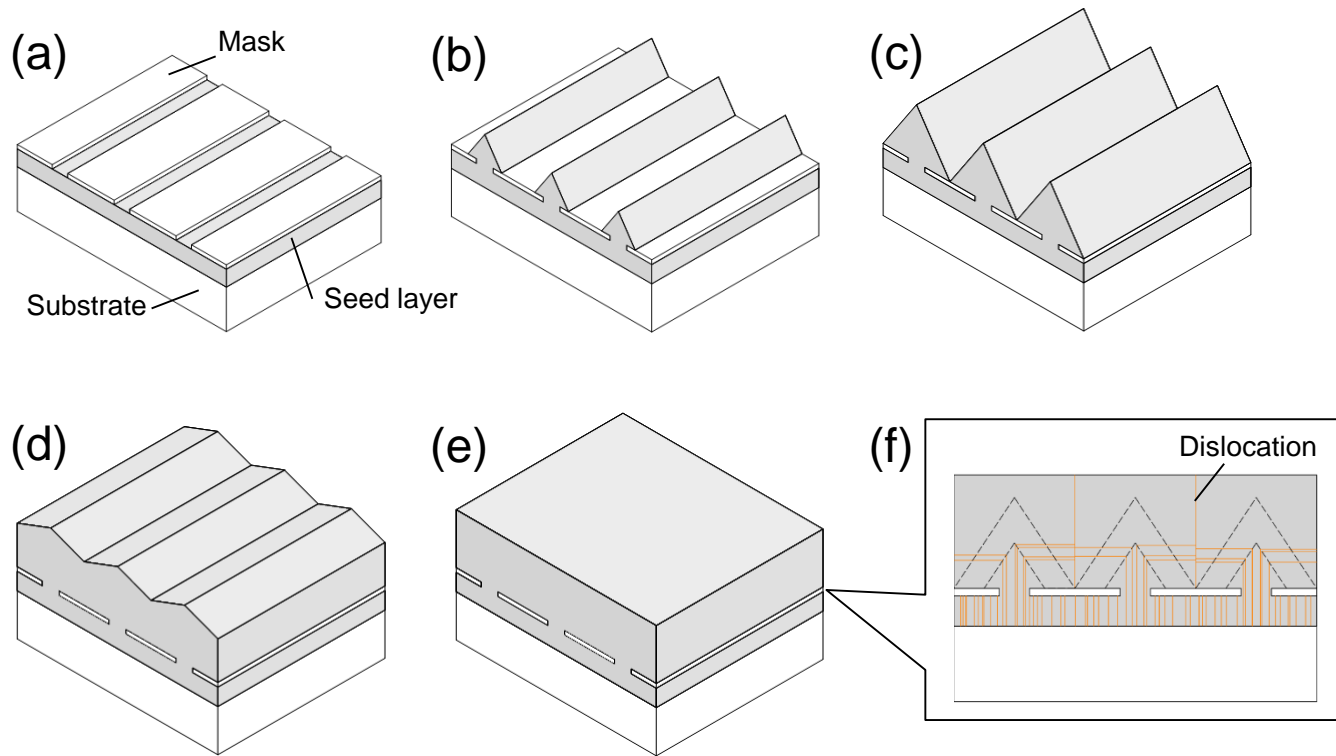
Figure 14

(a) Carrier concentration and (b) electron mobility at RT as functions of GeCl$_4$ bubbling rate. (c) Relationship between electron mobility and carrier concentration at RT for Ge-doped α-Ga$_2$O$_3$. Data from the literature [20] are also shown for comparison.
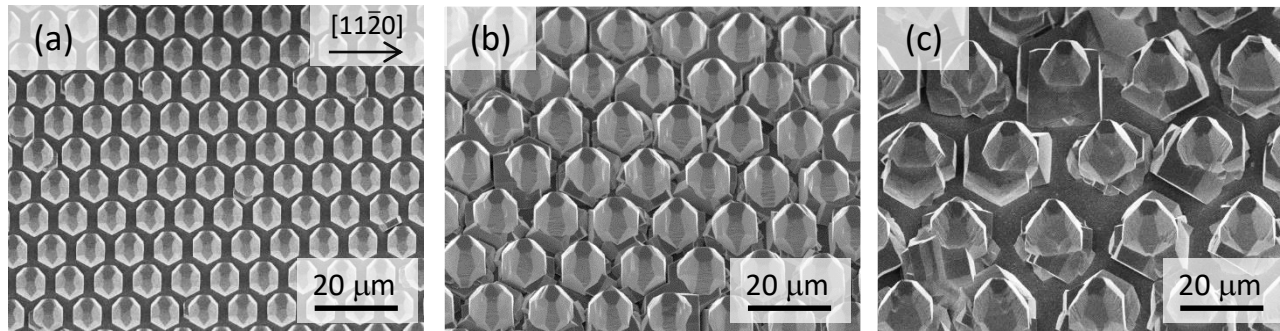
Figure 15

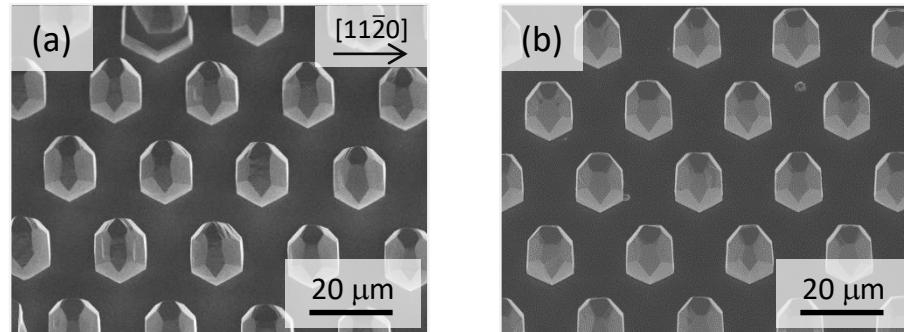(a) Carrier concentration and (b) electron mobility as functions of temperature.

Figure 16

(a) Mask, Substrate, Seed layer
(b)
(c)
(d)
(e)
(f) Dislocation
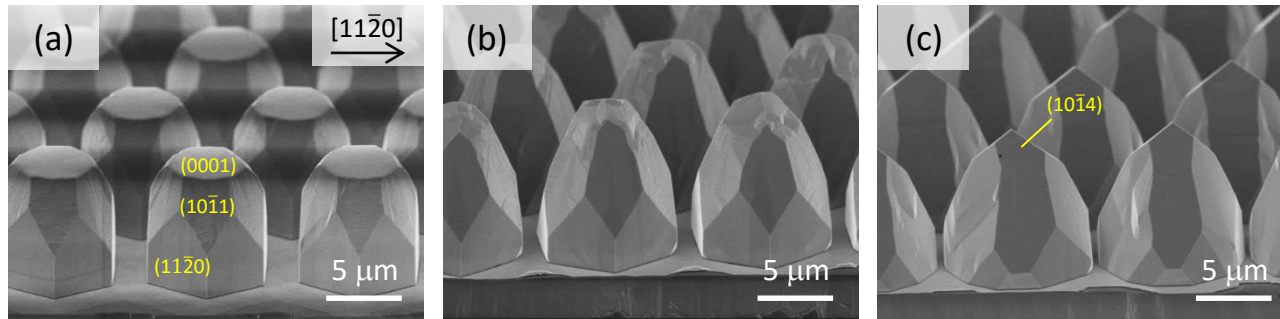
Procedure of FIELO technique.

Figure 17

SEM images of α-Ga$_2$O$_3$ islands grown on dot-patterned mask with window spacings of (a) 5 μm, (b) 10 μm, and (c) 20 μm (bird's eye view) [21].
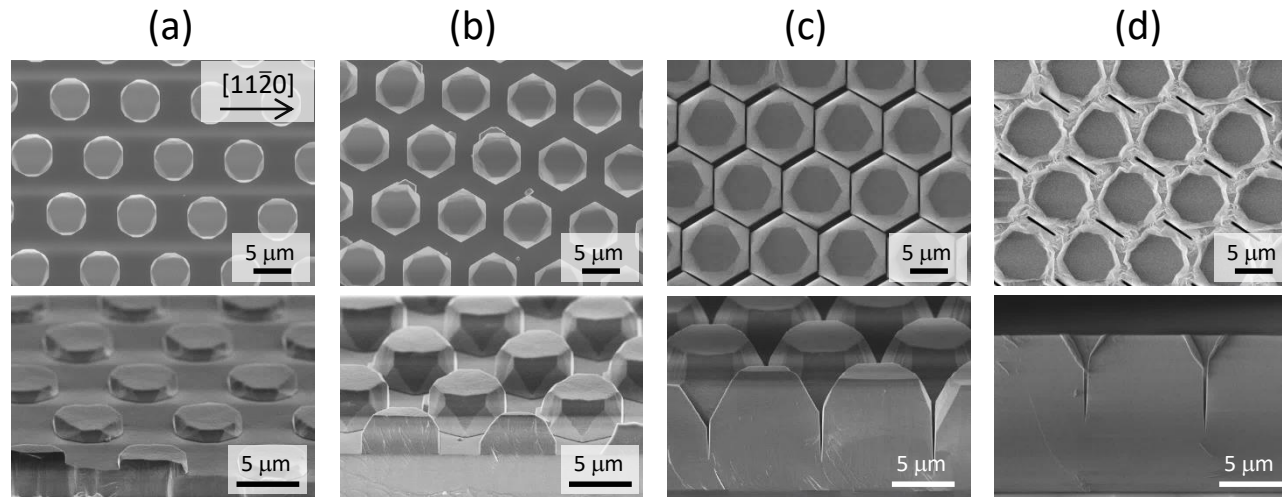
Figure 18

SEM images of α-Ga$_2$O$_3$ islands grown at nominal growth rates of (a) 7 μm/h and (b) 5 μm/h (bird's eye view) [21].
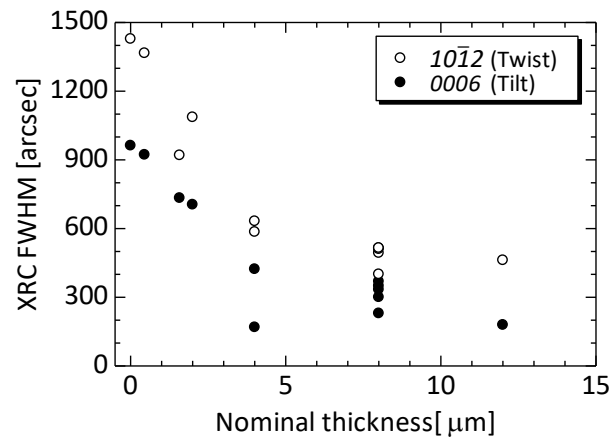
Figure 19

SEM images of α-Ga$_2$O$_3$ islands grown at (a) 540°C, (b) 500°C, and (c) 460°C (bird's eye view) [21].
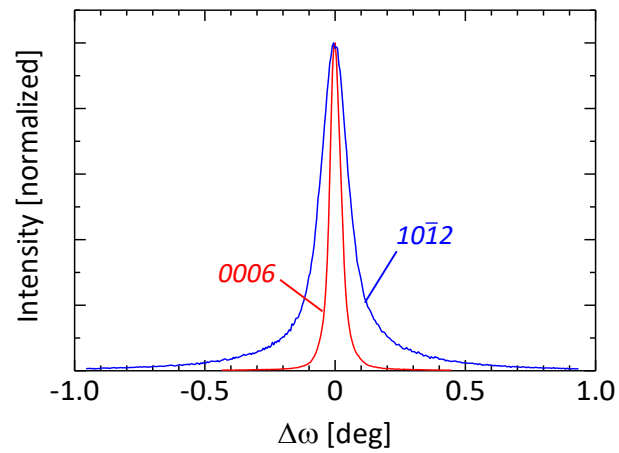
Figure 20

SEM images of α-Ga$_2$O$_3$ islands with nominal thickness of (a) 0.5 μm, (b) 1.6 μm, (c) 8 μm, and (d) 12 μm (plan-view and bird's eye view) [21].

Figure 21

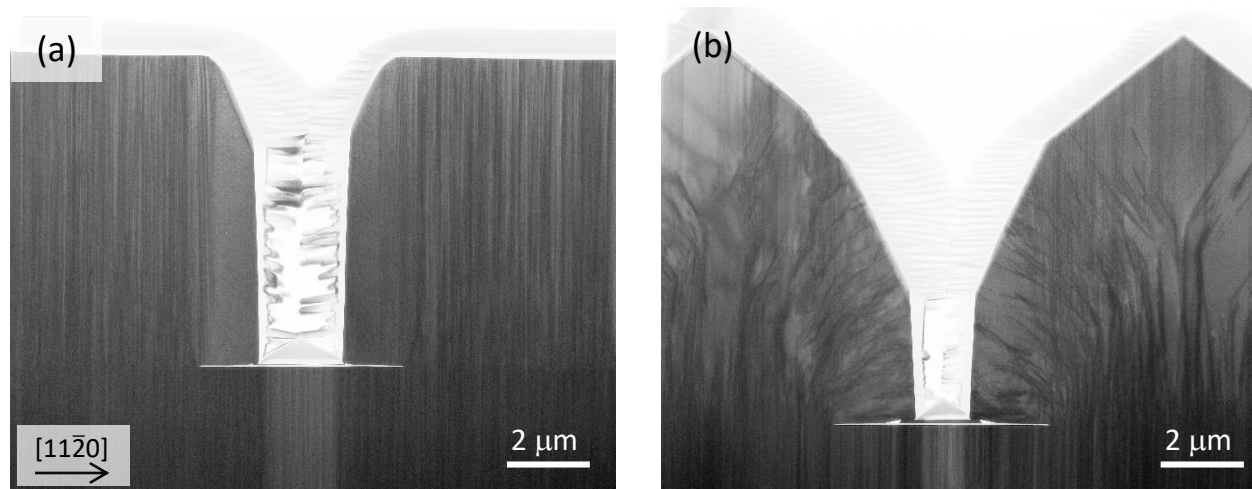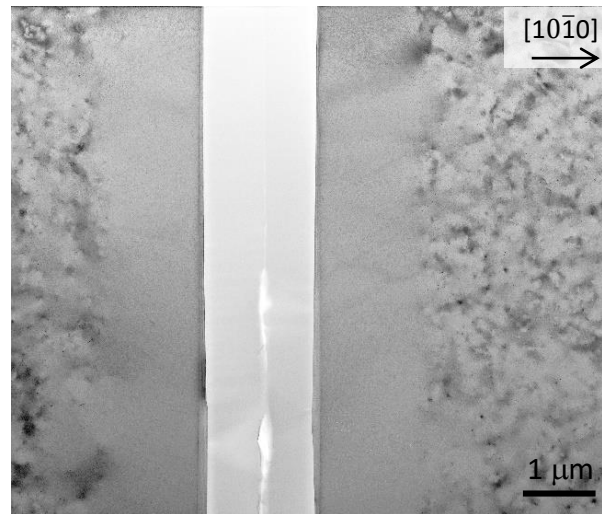XRC FWHMs of ELO-grown α-Ga$_2$O$_3$ as a function of nominal thickness [21].

Figure 22

XRC profiles of ELO-grown α-Ga$_2$O$_3$ with nominal thickness of 12 μm [21].
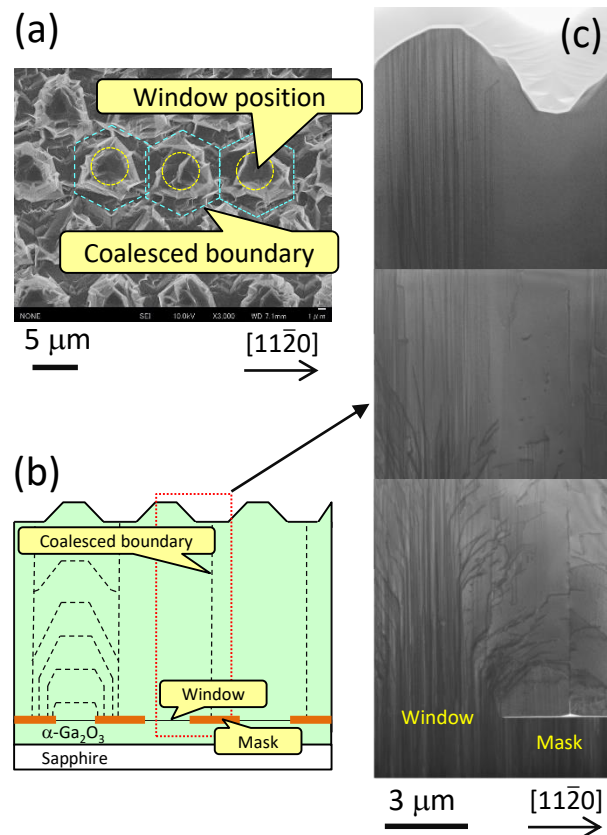
Figure 23

Cross-sectional TEM images of α-Ga$_2$O$_3$ islands grown at (a) 540°C and (b) 460°C.
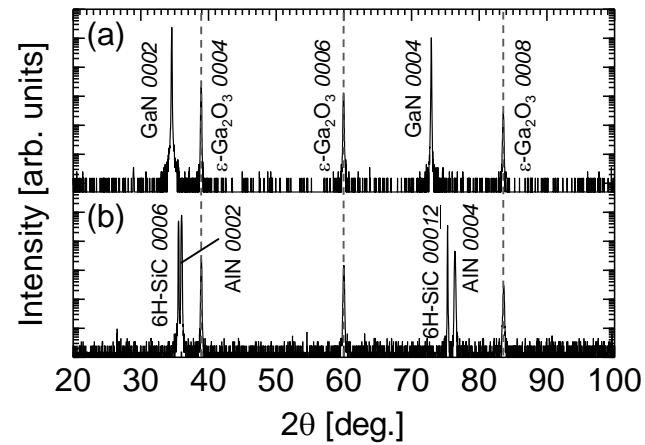
Figure 24

Plan-view TEM image of α-Ga$_2$O$_3$ stripes with well-developed (0001) plane [21].
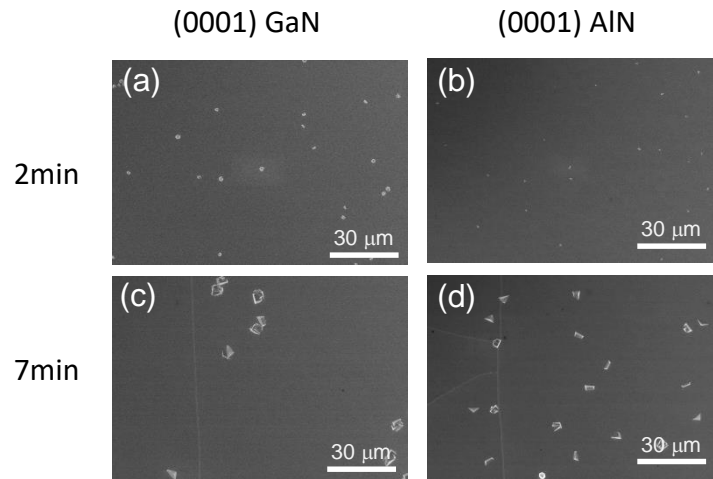
Figure 25

(a) Plan-view SEM image of a coalesced α-Ga$_2$O$_3$ film. (b) Schematic illustration of the cross section. (c) Cross-sectional TEM image of the film [21].
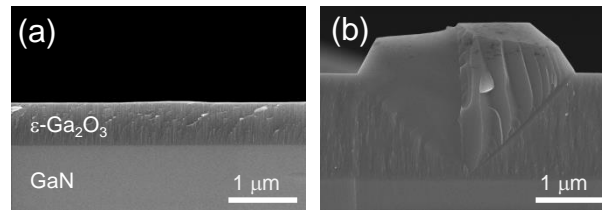
Figure 26

XRD ω–2θ scan profiles of ε-Ga$_2$O$_3$ layers grown on (a) (0001) GaN and (b) (0001) AlN [9].

Figure 27

(0001) GaN   (0001) AlN

(a)   (b)

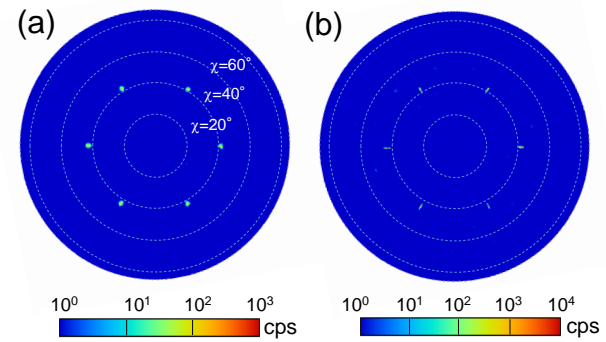2min

30 μm   30 μm

(c)   (d)

7min

30 μm   30 μm

Plan-view SEM images of ε-Ga$_2$O$_3$ layers grown on (0001) GaN and (0001) AlN with growth times of 2 and 7 min [9].
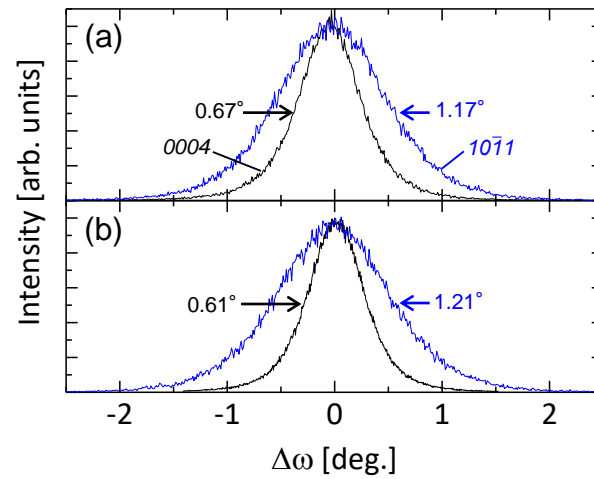
Figure 28

Cross-sectional SEM images of ε-Ga$_2$O$_3$ layers grown on (0001) GaN with growth times of (a) 2 min and (b) 7 min [9].
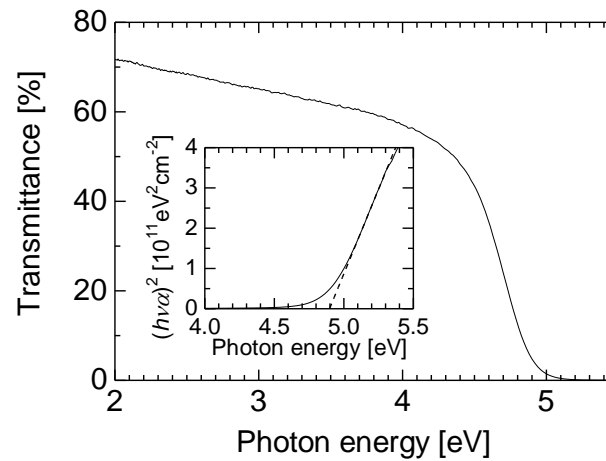
Figure 29

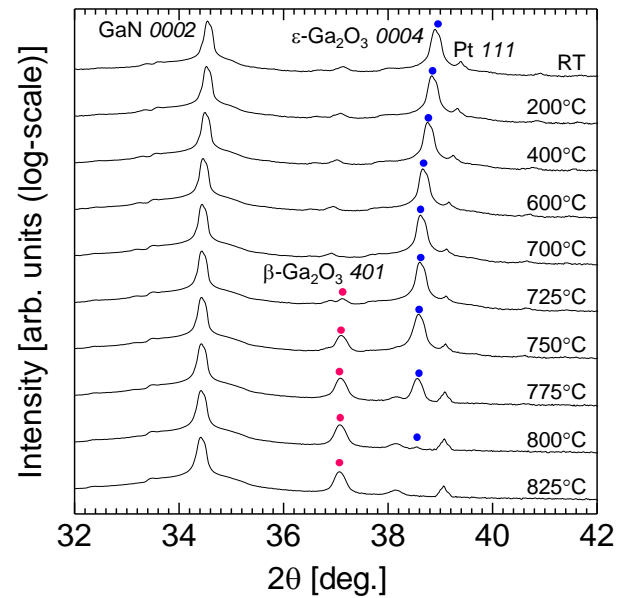X-ray pole figures (log scale) of (a) ε-Ga$_2$O$_3$ $10\bar{1}4$ and (b) GaN $10\bar{1}2$ [9].

Figure 30

XRCs of ε-Ga$_2$O$_3$ layers grown on (a) (0001) GaN and (b) (0001) AlN [9].

Figure 31

Transmittance spectrum of ε-Ga$_2$O$_3$. The inset shows the absorption coefficient in $(h\nu\alpha)^2$ vs. $h\nu$ [9].

Figure 32

XRD2θ–ω scan profiles for an HVPE-grown ε-Ga₂O₃ film measured at RT and elevated temperatures [9].